Investigation of Subsurface and Geological Structures Contributing to Collapse Sinkholes in Covered Karst Terrain, Northeast Thailand

Potpreecha Pondthai*, Rungroj Arjwech, Kannika Mathon, and Sutthipong Taweelarp

Department of Geotechnology, Faculty of Technology, Khon Kaen University, Khon Kaen 40002, Thailand

ARTICLE INFO

Received: 29 May 2023
Received in revised: 21 Sep 2023
Accepted: 25 Sep 2023
Published online: 19 Oct 2023
DOI: 10.32526/ennrj/21/20230131

Keywords:
Cover-collapse sinkholes/ Electrical resistivity tomography/ Rainfall/ Groundwater flow/ Phu Pha Man

*** Corresponding author:**
E-mail: potppo@kku.ac.th

ABSTRACT

This study focuses on covered karst terrain situated in Phu Pha Man District, Khon Kaen Province, Northeast Thailand, where records of collapse sinkholes are limited. Here, we investigate the subsurface characteristics and potential causes of sinkhole formation within this area using geophysical methods, hydrogeological techniques, and precipitation analysis. We collected field data by measuring groundwater levels, and conducting electrical resistivity tomography (ERT) surveys. We identified eight cover-collapse sinkholes of various shapes and sizes. Analysis of the groundwater flow indicated that the predominant flow direction runs from north to southeast. Examination of rainfall data showed a progressive increase in total rainfall on a yearly basis, with a significant precipitation event preceding the initial occurrence of sinkholes. The ERT results revealed the presence of highly resistive bedrock, water-saturated layers, and potential cavities. Notably, the tomograms indicated variations in resistivity values, suggesting the presence of irregular surfaces of limestone bedrock and weathered zones as characteristics of karst settings. Intense precipitation is a possible dominant trigger for the formation of the sinkholes. This study contributes to understanding sinkhole formation in karst environments and provides key information for hazard mitigation, not only in the Phu Pha Man District but also in areas with similar geological settings.

1. INTRODUCTION

Sinkholes are closed depressions with internal drainage observed on the surface, and formed by the presence of underground cavities or voids (Gutiérrez et al., 2014; Kaufmann et al., 2018). These voids gradually develop through physical-chemical weathering of underlying fractured bedrocks (Williams, 2008; Billi et al., 2016). Sinkholes are common in karst landscapes, characterized by the predominance of soluble rocks that can naturally dissolve through the circulation of groundwater within subsurface fractures (Heidari et al., 2011; USGS, 2018). When water infiltrates the soil, it combines with carbon dioxide released from organic matter, resulting in increased groundwater acidity. This process leads to the dissolution and erosion of soluble rocks in the shallow subsurface (Waltham et al., 2005; Kaufmann et al., 2011).

The formation sinkholes can be influenced by geological processes, climatic processes, and/or human activities (Kidanu et al., 2016; Youssef et al., 2016). Several factors can induce or accelerate sinkhole formation, such as intense rainfall events (Van Den Eeckhaut et al., 2007; Tufano et al., 2022), hydrological alterations (Doğan and Yilmaz, 2011; Pando et al., 2013), leakage from underground aqueducts (Richardson, 2013; di Santolo et al., 2018), and processes related to mining operations (Fidelibus et al., 2011; Ammirati et al., 2020).

Numerous studies have been conducted worldwide to investigate subsurface karst, deformation structures, and sinkhole development using various methods (e.g., Margiotta et al., 2012; Theron and Engelbrecht, 2018). Integrated geophysical surveys in karst environments have employed electrical, seismic, gravimetric, and electromagnetic methods to detect subsurface voids (Kruse et al., 2006; Kaufmann, 2014; Cueto et al., 2018). The analysis of groundwater flow paths has been shown to contribute to the creation of conceptual models for hydrogeological systems within

Citation: Pondthai P, Arjwech R, Mathon K, Taweelarp S. Investigation of subsurface and geological structures contributing to collapse sinkholes in Covered Karst Terrain, Northeast Thailand. Environ. Nat. Resour. J. 2023;21(6):513-523. (https://doi.org/10.32526/ennrj/21/20230131)

karst areas (Nam et al., 2020; Al-Halbouni et al., 2021). Long-term geophysical monitoring and precipitation records have been utilized to gain insights into the interaction between subsurface conditions and dynamics of infiltration within karst systems (Watlet et al., 2018).

Sinkhole collapses in Thailand which occur in areas characterized by karst landforms such as limestone, gypsum, or salt, pose significant threats to human lives and property (DMR, 2011). Extensive research has been conducted to investigate the mechanisms underlying sinkhole development in karst regions of Thailand, employing various approaches including geomorphology and geophysics (Furukawa and Pichai, 1989; Giao et al., 2011; Yordkayhun, 2021). However, there remains a paucity of studies specifically focused on the causes of shallow collapses, particularly within rock salt strata (Satarugsa, 2011) and carbonate rocks (Arjwech et al., 2021) in northeast Thailand.

This study aims to examine the potential factors contributing to the occurrence of sinkhole hazards in a buried karst area where such events have not been previously documented. On April 19th, 2021, unexpected events unfolded when the Phu Pha Man district experienced the sudden emergence of two massive collapse sinkholes. Subsequently, six additional sinkholes were discovered, as indicated in the report by DMR (2021). Our aim is to gain a comprehensive understanding of the underlying causes and mechanisms associated with sinkhole formation in the area. To achieve our research objective, we employ the geophysical method of Electrical Resistivity Tomography (ERT) to investigate the subsurface characteristics of the sinkhole-affected region. In addition, we utilize supportive data, including measurements of groundwater levels and historical precipitation records. By combining these approaches, our findings could provide valuable insights for identifying sinkhole-prone areas, which contribute to enhancing hazard mitigation planning.

2. METHODOLOGY

2.1 Geological setting and study site

The Phu Pha Man District is located on the westernmost part of Khon Kaen Province and is geologically situated on the western edge of the Khorat Plateau (Figure 1). The district's geological setting comprises mostly sedimentary rocks deposited during the upper Paleozoic to Mesozoic periods (DMR, 2007; Booth and Sattayarak, 2011). Additionally, there are sparse occurrences of extrusive igneous rocks from the Triassic to Permian age (PTrv). The Permian rocks primarily consist of shallow-marine deposits and epeiric carbonate platforms, forming karst landforms. These rocks are represented by the Ratburi (P1) and Saraburi (Ps) groups, found in the northeastern and middle parts of the district, respectively. Lithological logs indicate that the Ratburi group consists of thin- to medium-bedded limestone intercalated with thin-bedded grey shale (Chonglakmani and Sattayarak, 1984; Chaodumrong et al., 2007). The Saraburi group is characterized by fossiliferous limestone, shale interbedded with limestone, shale, sandstone, siltstone, and tuffaceous sandstone (Ueno and Charoentitirat, 2011). The Khorat Plateau Basin was formed as a result of the collision between the Sibumasu (Shan-Thai) and Indochina continental blocks during the Permo-Triassic period (Minezaki et al., 2019). This collision led to the uplift and profound erosion of Permian carbonate platforms during the Indosinian I Event (Booth and Sattayarak, 2011). Subsequently, the Khorat Group was deposited from the Triassic to Cretaceous periods and primarily consists of terrigenous sediments. In the Phu Pha Man District, the Huai Hin Lat (TRhl), Nam Pong (Trnp), and Phu Kradung (Jpk) formations are present. The depositional environments of the extensive limestone formations overlying carbonate units in this area are similar to those in Saraburi Province, which has experienced a cluster of sinkhole collapses (DMR, 2005; Ponta et al., 2013).

The study site is situated on the eastern border of the Phu Pha Man District, ~110 km northeast of Khon Kaen City. The site encompasses an area of ~2 km^2, spanning across the Phu Pha Man and Huai Muang Sub-Districts (in Figures 1 and 2, highlighted with a yellow-black rectangle). Geological formations in the area include massive limestone boulders located in the western section and clast-supported conglomerate outcrops found in the eastern part of the site. The surficial layer is predominantly covered by unconsolidated soils consisting of Quaternary fluvial deposits, underlain by rocks from the Khorat group. The soils in the area are classified by the Land Development Department (2005) as a mixture of sandy clay loam and silty clay. The land in this area is extensively utilized for agricultural purposes, primarily for sugarcane and rice cultivation. A limestone quarry is also located nearby, within 2 km from the study site.

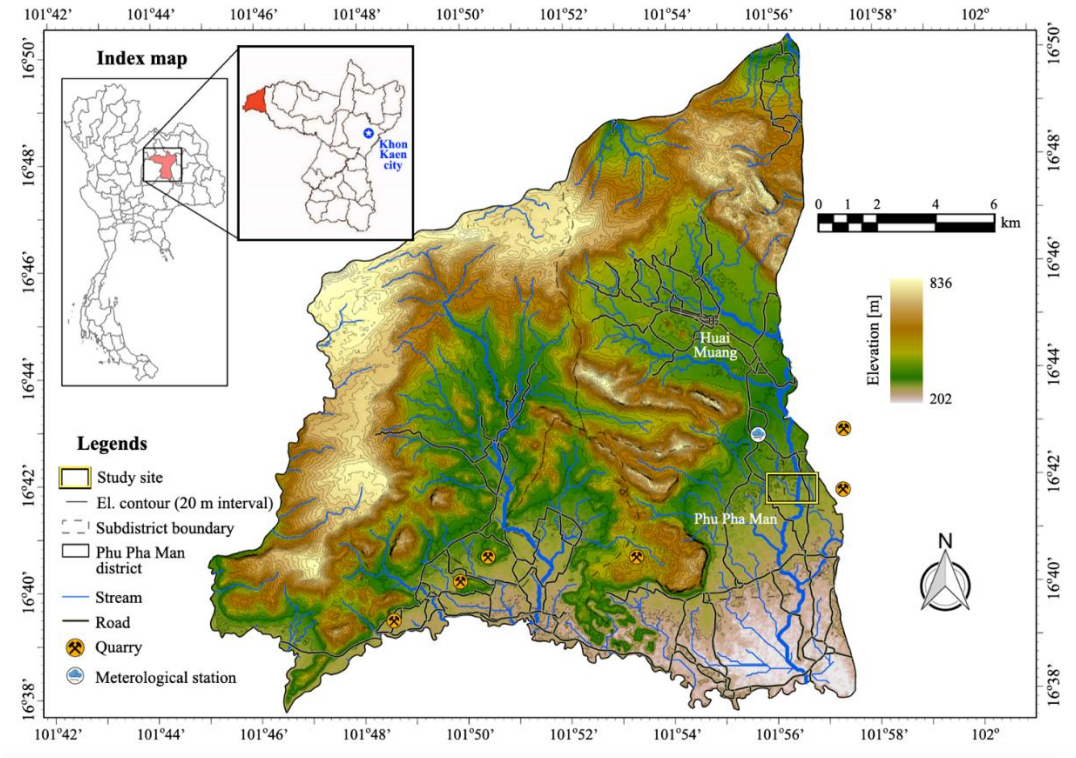

Figure 1. Topographic map of Phu Pha Man District. An index map shows the location of Khon Kaen Province in Northeastern Thailand. The study site is marked by a yellow-black rectangle.

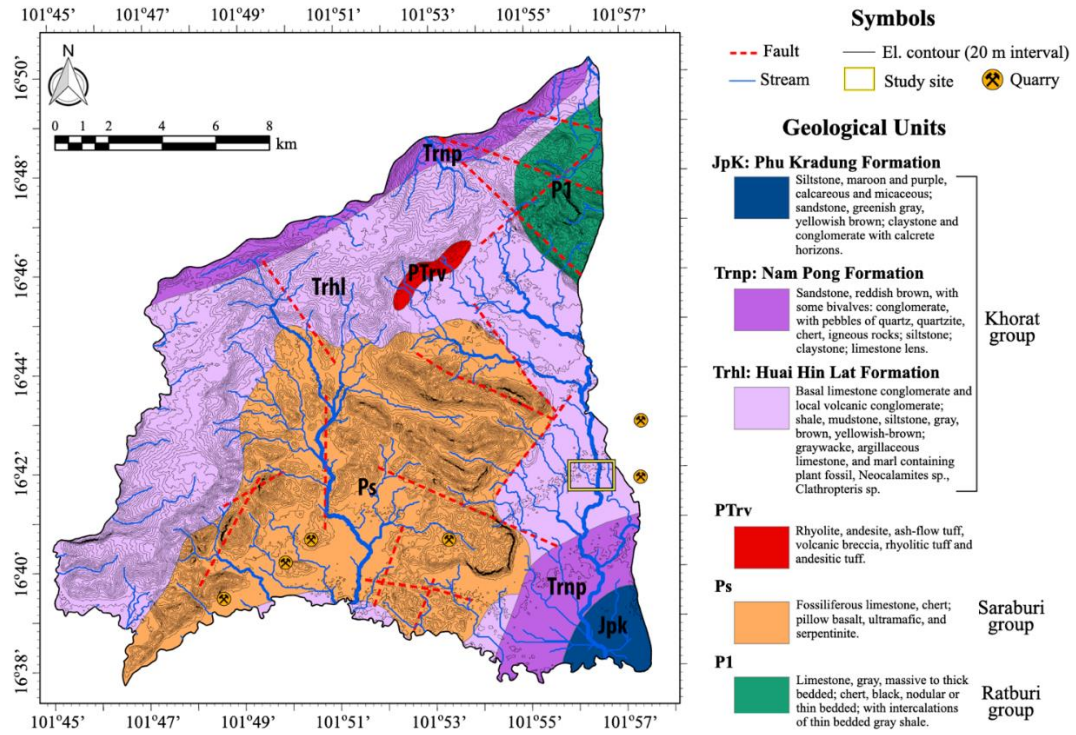

Figure 2. Geological map of Phu Pha Man District and locations of quarries (Modified from DMR (2007))

2.2 Field data acquisition

We began visiting in the middle of 2021 to verify and map subsidence features identified through preliminary aerial imagery study. Further field inspections then conducted to gather more detailed information. Based on the findings from the initial site

visits, preferred locations for ERT surveys were determined. Additionally, another round of site visits took place from late 2021 to early 2022 to perform groundwater level measurements and carry out geophysical fieldwork.

Transient groundwater level measurements were conducted within the study site during the crop harvesting period (December 2021 to January 2022). A total of 11 local wells, primarily drilled for agricultural purposes, were identified and distributed across the study area. At each well location, the depth to the local groundwater table was measured using a flat tape water level indicator, and the precise coordinates were recorded using RTK GNSS positioning systems. Subsequently, the collected hydraulic head data from the field measurements were utilized to generate a groundwater flow contour map.

In addition to water table measurements, rainfall data from the years 2019 to 2021 were utilized as supplementary information for this study (Upper Northeastern Meteorological Center, 2022). The data was obtained from a meteorological station located in the Huai Muang Sub-District, ~2 km northwest of the study site (Figure 1).

ERT is a geophysical method that provides an image of the electrical resistivity structure in a vertical plane beneath a linear array of metal electrodes inserted in the ground and connected together by a multi-core cable (Everett, 2013). By measuring the voltage developed across pairs of electrodes during current injections and withdrawals, information about the electrical resistivity spatial distribution can be obtained. In this study, ERT data was collected using the IRIS SYSCAL Pro instrument from January to February 2022. A total of nine 2D ERT profiles, designated as PPM_1 to PPM_9, were conducted in the vicinity of the observed surficial collapses, covering a combined array length of 1,755 m (Figure 3). The ERT survey utilized a dipole-dipole measurement protocol because it is the most effective array for karst mapping, as discussed in Zhou et al. (2002). A typical electrode spacing of 5 m was used, except for PPM_6 to PPM_9, which had an electrode spacing of 2.5 m. The positions and elevations of the electrodes were accurately acquired using RTK GNSS positioning systems. Most ERT profiles were oriented approximately in the N-S direction, perpendicular to the trend of the observed sinkholes identified during the preliminary field investigation. There is only one profile (PPM_3) that extended from W to E. The selection of each ERT survey location attempted to capture a broad subsurface image, aiding in the identification of sinkhole-related features. The acquired ERT data were processed using topographic reconstruction methods implemented in Res2DInv software. The finite-element algorithm was selected to discretize and optimize a geoelectrical model. The L-1 norm inversion method was used to minimize the sum of absolute derivation between the measured and the calculated apparent resistivities for each iteration.

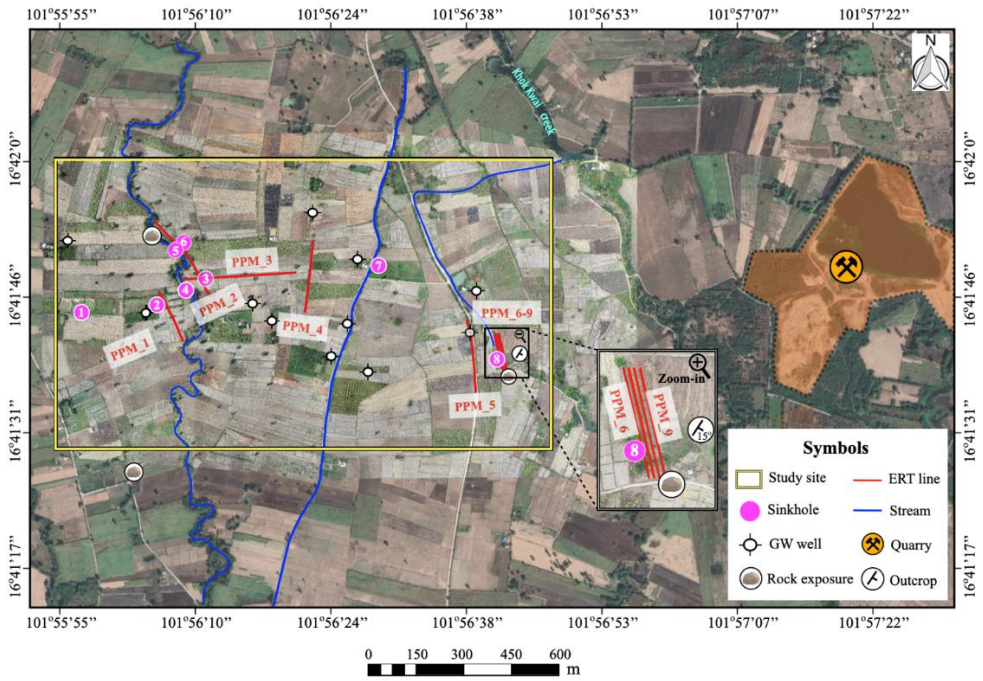

Figure 3. An overlay aerial photograph on satellite imaginary showing details of the study site

3. RESULTS

3.1 Sinkhole formation

During site visits in 2021, field investigations and physical measurements were conducted within an area of ~2 km^2. As a result, eight cover-collapse sinkholes were identified (Figure 4(a-d)). Among these sinkholes, three exhibited partial filling with water at varying levels. The surficial sinkholes displayed a range of shapes, transitioning from nearly circular to irregular as their size increased. Detailed dimensions of all sinkholes are provided in Table 1. The sinkholes can be categorized into two groups: (1) three collapses located further inland, distanced from surface water drainages in the western parts of the site, referred to as sinkholes #1, #2, and #3; (2) five relatively larger sinkholes situated near streams or irrigation waterways, designated as sinkholes #4 to #8. In the study site, the frequency of sinkhole formation is increasing, as several additional collapses were reported by local residents after the harvesting period in early 2022. However, this study does further discuss these recent sinkholes.

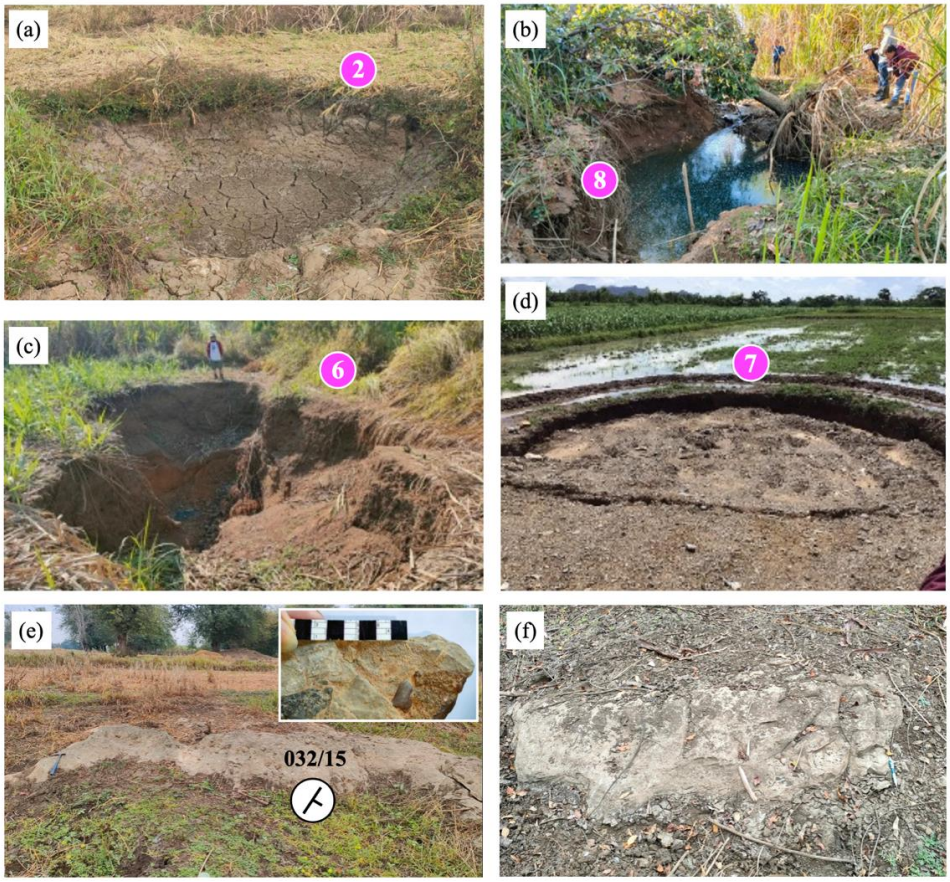

Figure 4. (a-d) Examples of existing sinkholes; (e) Conglomerate outcrop found in the east; (f) Massive limestone boulder exposed in the west

Table 1. Dimensions of collapse sinkholes

Group	Sinkhole No. #	Width (m)	Length (m)	Depth (m)	Estimated volume (m^3)
1	1	8.6	9.4	Filled* (3.2)	203.17
	2	0.7	0.7	0.4	0.15
	3	4.2	5.1	Filled* (1.2)	20.19
2	4	4.0	5.5	Flooded	N/A
	5	8.7	9.3	Partially flooded (>4)	>254.17
	6	3.1	10.0	5.2	126.61
	7	7.0	7.8	Filled	N/A
	8	5.0	6.0	Flooded	N/A

*The depth acquired from geological hazard report by DMR (2021).

3.2 Groundwater flow and rainfall

Figure 5 illustrates the distribution of groundwater wells within the study site, with a noticeable sparsity observed in the western region compared to the middle and eastern areas. The hydraulic head data indicates that higher groundwater levels are predominantly located in the north and northwest parts of the site. Consequently, groundwater generally flows from the N to SE direction in the western to middle sections, gradually transitioning to W to E flows in the eastern part. Additionally, the groundwater elevation map reveals larger gradients in the eastern part of the site.

Figure 6 presents the precipitation records obtained from the meteorological station near the study site during 2019-2021. The pattern of monthly accumulated rainfall does not appear to exhibit a clear systematic trend over the three-year period. However, the total amount of rainfall clearly increased over the study period. In particular, an exceptional heavy rainfall event or monsoon occurred in April 2021, preceding the regular rainy season (typically in mid-May). During this event, the precipitation exceeded 200 mm, a significant increase from the ~5 mm recorded in March of the same year. These sudden and intense rainfall events coincided with the initial occurrence of collapse sinkholes in the area. Additionally, a prolonged dry period with limited rainfall from November 2020 to March 2021, combined with groundwater pumping for agricultural activities, contributed to the decline of the groundwater table in the area.

3.3 ERT results

2D tomographic images were arranged into the fence diagram in order to visualize the continuity of the subsurface structures in the study area (see Figures 7 and 8). Inverted ERT sections (tomograms), generated after six iterations of the reconstruction algorithm, exhibited misfits of less than 10%, indicating a good fit to the measured data. Three principal zones can be broadly identified in the tomograms. The surficial layer of the tomograms exhibited low resistivity values (1-120 Ωm), represented by dark blue to dark green colors, which are interpreted as overburden fluvial sediments. The moderate resistivity zone (120-1,200 Ωm), appearing at a depth of ~5-10 m in all sections, likely indicates water-saturated layers and/or weathered rocks. The zone of high resistivity (>1,200 Ωm), depicted by orange to dark purple colors, corresponds to the sedimentary bedrock.

ERT profile PPM_1 was deployed near the collapse sinkhole #2 (top left panel in Figure 7). The tomogram for this profile does not show any indication of highly resistive bedrock within the investigated depth of 35 m. However, a high resistive anomaly was observed at the location of 85-100 m, marked with a '?' symbol, which is likely caused by an air-filled cavity. ERT profile 2 exhibits a relatively wide range of bulk resistivity values down to a depth of 60 m and

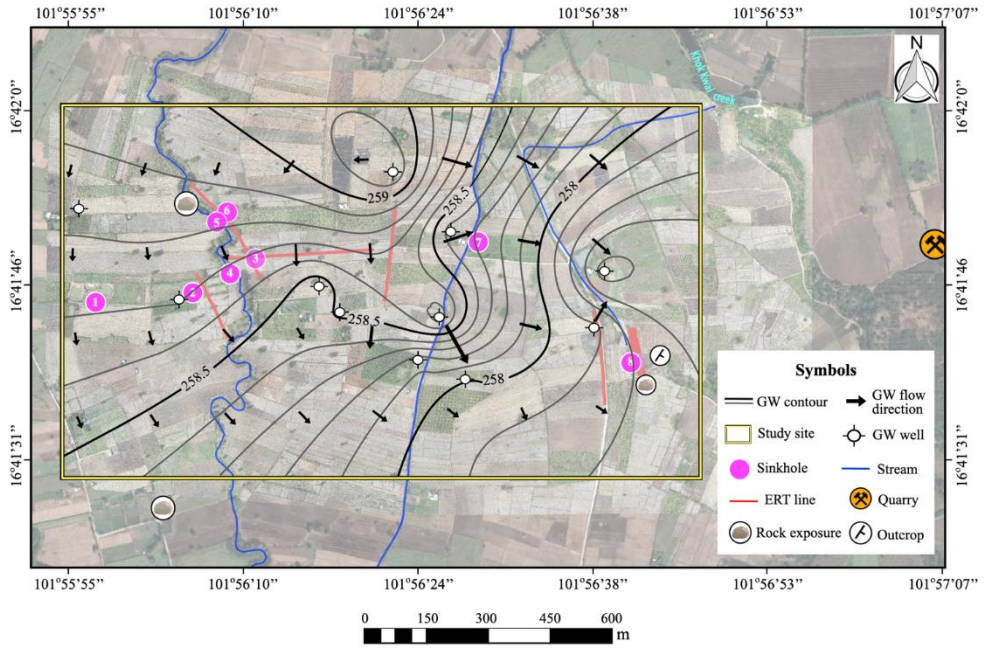

Figure 5. Groundwater (GW) elevation map of study site. Note that the length of arrow is an indicative of flow direction and proportional to hydraulic gradient at each location.

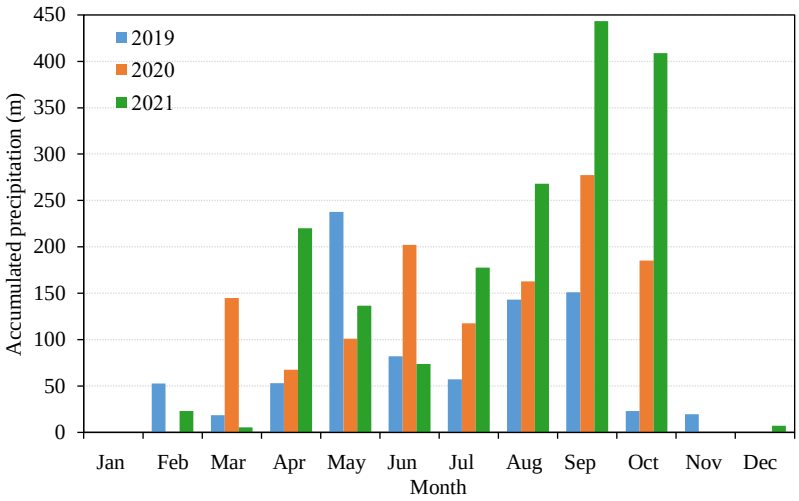

Figure 6. Monthly accumulated rainfall during 2019-2021 at the meteorological station located near the study site

shows a high spatial distribution of Earth resistivity. In the southern half of the section, there are notably high resistivity values, starting at around 10 m depth, which can be interpreted as limestone bedrock based on the presence of exposed rocks nearby. A water-saturated zone is identified in the middle of the transect, extending from depths of 10-30 m, coinciding with the partially flooded area near sinkhole #5. Additionally, a moderate resistive anomaly was observed at a location of 200 m (marked as '??' symbol), which is interpreted as a cavity filled with water-saturated soils. ERT profile PPM_3 intersects profile PPM_2 at location ~55 m on PPM_3 and ~60 m on PPM_2. This section is located adjacent to sinkhole collapse #3 at a location of 60 m and does not exhibit any indication of electrical subsurface anomalies. The top layer in the eastern section of profile PPM_3, spanning from the surface to a depth of ~5 m, corresponds to variably saturated topsoil of a paddy rice field. Along the transect, between locations of 80-260 m, a highly weathered zone is observed with a moderate range of resistivity values, extending from 15-65 m in depths. The highly resistive bedrock in the eastern half of the section, below 20 m, indicates the continuity of an underlying unit that dips eastward. ERT profile PPM_4, a distinct irregular shape was observed at depths around 10-30 m of the substratum surface, which is indicative of karst settings. The presence of uneven surfaces can be attributed to spatial variations in lithology and differential rates of weathering within the limestone bedrock.

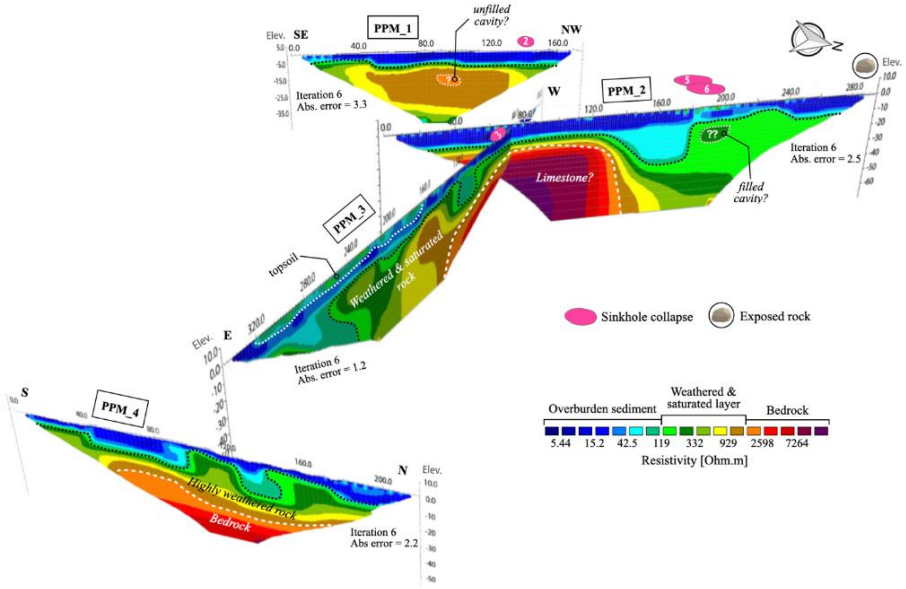

Figure 7. Geoelectrical resistivity fence diagram of 2D inversion tomograms shows subsurface features and inferred cavities in the western part of the study site.

Figure 8 presents the fence diagram illustrating the ERT inversion images of PPM_5, PPM_6, PPM_7, PPM_8, and PPM_9, which cover the eastern part of the study site. Note that these profiles extend in SE to NW direction. The interpreted bedrock in profile PPM_5 appears to be relatively shallower but more resistive when compared with the profiles in the western part of the study area (PPM_2, PPM_3, and PPM_4). In this section, the top layer shows a slightly increased thickness and higher conductivity in the NW part. Similarly, the middle layer, within the moderate resistivity range, appears to be thicker, indicating increased weathering of rocks in the NNW half of the transect. Furthermore, a zone of low resistivity, indicating a highly weathered layer, is observed in the SE part of the transect, specifically at locations 40-60 m, extending from the surface to depths of 20 m. This low resistivity zone is likely caused by loam soils with a relatively high water content. Four geoelectrical tomograms, namely PPM_6 to PPM_9, were conducted with a length of 115 m to reach investigation depth of ~25 m. The electrode separation for this measurement protocol was 2.5 m, and the survey lines were parallel to each other with a spacing of 5 m. Profile PPM_6 was positioned ~100 meters east of profile PPM_5. This transect was located within a close proximity of less than 5 m east of the flooded open collapse #8, which can be seen at the location ~35 m along the transect (second panel from the top in Figure 8). Between the locations of 40-50 m, an irrigation drainage was identified, which serves to convey surface water to the sinkhole (water ingress). The tomograms PPM_7, PPM_8 and PPM_9 exhibit characteristics similar as the one observed in PPM_6. In these transects, a zone characterized by low resistivity values, indicated by the dashed gray lines, is more pronounced in the southwestern half. Furthermore, this zone appears to become more continuous and slightly more resistive across adjacent tomograms, suggesting a potential groundwater flow path in the west to east direction. Notably, the water from the drainage directly feeds sinkhole #8 and cannot be traced from the surface. In contrast, the resistivity of the uppermost layer in the northwestern half decreases as the ERT surveys move eastward, indicating an increase in water content within the overburden soils. Additionally, the underlying bedrock in this half of the transects (PPM_6 to PPM_9) appears to be less weathered in the eastward direction. Scattered boulders were observed on the surface in the southwestern parts of profiles PPM_7 to PPM_9. These rock exposures were characterized as conglomerate, predominantly composed of limestone clasts. Additionally, a conglomerate outcrop located ~60 m east of profile PPM_5 was measured (see Figure 4(e)). The outcrop exhibited a NE-SW orientation with a dip of 15° in the SE direction (032/15).

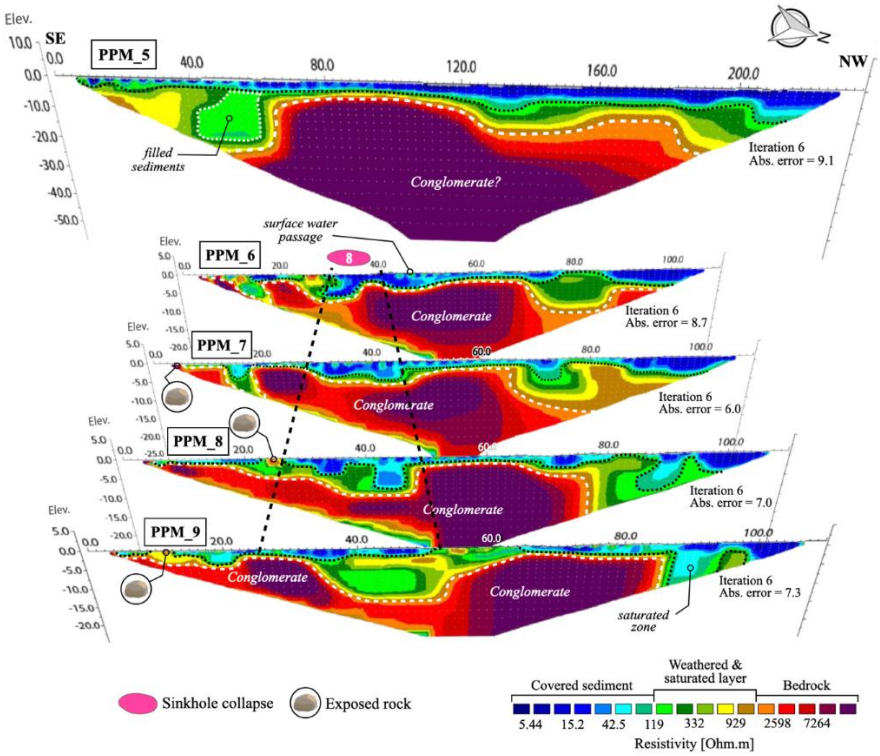

Figure 8. Fence diagram of 2D ERT inversion images shows subsurface features in the eastern part of the study site.

4. DISCUSSION

The findings of this study suggest that the presence of continuous large-scale cavities related to fractures in the bedrocks of the study area is unclear based on geophysical results. However, based on the prevailing lineation trend of existing surface collapses, it is speculated that fracture zones may extend in a west-east direction. Additionally, the results indicate that the triggering factors contributing to sinkhole collapses differ from others found within northeast Thailand. Arjwech et al. (2021) mentioned that anthropogenic factors such as quarry dewatering and blasting mainly influence the occurrence of sinkholes in Nong Bua Lamphu Province.

The upward migration of voids in the cohesive covering soil, characterized by its high clay content, occurs above pre-existing dissolution fissures located in the limestone bedrock through roof breakdown or erosion (Ayalew et al., 2004; Sauro et al., 2019). The dry season from November 2020 to March 2021 led to a decrease in groundwater levels within the study site, resulting in a loss of buoyant support in the cavity's roof. During the period before the onset of the regular rainy season, particularly in April 2021, the abrupt change in precipitation at the site suggests a potential increase in overburden weight due to rainfall infiltration and recharge from nearby surface drainages (Van Den Eeckhaut et al., 2007; Theron and Engelbrecht, 2018). The combination of increased water input to the ground and a decline in the water table may accelerate the processes of arch cavity growth and upward migration (Youssef et al., 2020). As the cavities progressively grow, they eventually breach the ground surface (Tufano et al., 2022), observed as depressions resulting from the first surficial collapses in April 2021. This drastic increase in water percolation, a result of high-intensity rainfalls continuing from May to October in the same year, is believed to be a cause of subsequent sinkholes in the study site.

The underground mining activities in the nearby limestone quarry could also potentially contribute to the formation of sinkholes (Richardson, 2013; Ammirati et al., 2020). Historical aerial imagery reveals that the quarry was operational from 2018 until the end of 2021, with the initial pit being filled with water. The excessive dewatering process associated with quarry operations may have led to a decline in regional groundwater levels within the aquifer (Gutiérrez et al., 2014). This, in turn, could have influenced the occurrence of sinkholes in the study area. The hydraulic head mapping conducted in this study indicates that the groundwater generally flows in the region is towards the western area, suggesting that the quarry serves as a potential recharge area.

Although the acquired geophysical data did not provide a clear indication of the presence of cavernous karst systems or connected fractures in this specific location, the sinkhole-prone area, where significant surface collapses are likely to occur, appears to be in close proximity to surface water drainages, such as natural creeks and irrigation canals.

5. CONCLUSION

This study demonstrates the effectiveness of using the geophysical ERT method, along with hydrogeological mapping and precipitation records, to investigate areas affected by sinkholes. In this study, we focused on imaging the subsurface structures within the Huai Hin Lat carbonate formation, which is covered by Quaternary fluvial deposits in the eastern part of the Phu Pha Man District, Northeastern Thailand. Groundwater flow analysis indicated flow directions from north to southeast in the western to middle sections of the site, transitioning to west to east flows in the eastern part. Rainfall data showed an increasing trend in precipitation over the study years, and a heavy rainfall event in April 2021 coincided with the initial occurrence of sinkholes. The results of the ERT inversion revealed valuable information about the depths, ranging from 25-60 m, and coverage area of ~2 km^2. These results also unveiled distinct spatial variations in geoelectrical resistivity, providing insights into the different degrees of weathering found in karst terrains. We also identified zones of cover materials that host cavities and have the potential to lead to collapses. The occurrence of collapses in this area can be attributed to a combination of factors, including the presence of local-scale cavities in heterogeneous cover layers above the Triassic limestone, unusually high precipitation events, the infiltration of surface water, and potentially the dewatering activities associated with the nearby limestone mine. With the limited data we have acquired, we suggest that intense rainfall could be the dominant triggering factor that has the most influence on sinkhole development. This is due to the unclear connectedness of subsurface cavities within the karst system, a lack of assessable dewatering impact, and an uncertainty regarding the spatial concentration of

collapses coinciding with surface drainages. To mitigate potential future collapses, it may be necessary to implement regulatory measures limiting further intensification of land use and groundwater withdrawal.

ACKNOWLEDGEMENTS

This research is funded by the Young Researcher Development Project of Khon Kaen University Year 2022. The authors thank the undergraduate geotechnology students' class of 2022 for assisting with the field data acquisition.

REFERENCES

Al-Halbouni D, Watson RA, Holohan EP, Meyer R, Polom U, Dos Santos FM, et al. Dynamics of hydrological and geomorphological processes in evaporite karst at the eastern Dead Sea: A multidisciplinary study. Hydrology and Earth System Sciences 2021;25(6):3351-95.

Ammirati L, Mondillo N, Rodas RA, Sellers C, Di Martire D. Monitoring land surface deformation associated with gold artisanal mining in the Zaruma City (Ecuador). Remote Sensing 2020;12(13):Article No. 2135.

Arjwech R, Ruansorn T, Schulmeister M, Everett ME, Thitimakorn T, Pondthai P, et al. Protection of electricity transmission infrastructure from sinkhole hazard based on electrical resistivity tomography. Engineering Geology 2021;293:Article No. 106318.

Ayalew L, Yamagishi H, Reik G. Ground cracks in Ethiopian Rift Valley: Facts and uncertainties. Engineering Geology 2004;75(3-4):309-24.

Billi A, De Filippis L, Poncia PP, Sella P, Faccenna C. Hidden sinkholes and karst cavities in the travertine plateau of a highly-populated geothermal seismic territory (Tivoli, central Italy). Geomorphology 2016;255:63-80.

Booth J, Sattayarak N. Subsurface carboniferous - Cretaceous geology of NE Thailand. In: Ridd MF, Barber AJ, Crow MJ, editors. The Geology of Thailand. United Kingdom: Geological Society of London; 2011. p. 185-222.

Chaodumrong P, W XD, Shen SZ. Permian lithostratigraphy of the Shan-Thai Terrane in Thailand: Revision of the Kaeng Krachan and Ratburi groups. Proceedings of International Conference on Geology of Thailand: Towards Sustainable Development and Sufficiency Economy; 2007 Nov 21-22; Department of Mineral Resources, Bangkok: Thailand; 2007.

Chonglakmani C, Sattayarak N. Geological Map of Phetchabun Province, Scale 1:250,000. Bangkok, Thailand: Department of Mineral Resources; 1984.

Cueto M, Olona J, Fernández-Viejo G, Pando L, López-Fernández C. Karst-induced sinkhole detection using an integrated geophysical survey: A case study along the Riyadh Metro Line 3 (Saudi Arabia). Near Surface Geophysics 2018;16(3):270-81.

di Santolo AS, Forte G, Santo A. Analysis of sinkhole triggering mechanisms in the hinterland of Naples (Southern Italy). Engineering Geology 2018;237:42-52.

Doğan U, Yılmaz M. Natural and induced sinkholes of the obruk plateau and karapınar-hotamış plain, Turkey. Journal of Asian Earth Sciences 2011;40(2):496-508.

Department of Mineral Resources (DMR). Risk Map of Subsidence Sinkhole in Khon Kaen Province. Bangkok, Thailand: Department of Mineral Resources, Ministry of Natural Resources and Environment; 2005.

Department of Mineral Resources (DMR). Geologic map of Khon Kaen Province, Scale 1:1,000,000. Bangkok, Thailand: Department of Mineral Resources, Ministry of Natural Resources and Environment; 2007.

Department of Mineral Resources (DMR). Handbook of Reducing the Impact Disaster. Bangkok, Thailand: Department of Mineral Resources, Ministry of Natural Resources and Environment; 2011 (in Thai).

Department of Mineral Resources (DMR). Report on sinkhole inverstigation in Phu Pha Man District, Khon Kaen Province [Internet]. 2021 [cited 2021 May 20]. Available from: https://phupaman.go.th/public/list/data/detail/id/2930/menu/1554/ (in Thai).

Everett ME. Near-Surface Applied Geophysics. New York, USA: Cambridge University Press; 2013.

Fidelibus MD, Gutiérrez F, Spilotro G. Human-induced hydrogeological changes and sinkholes in the coastal gypsum karst of Lesina Marina area (Foggia Province, Italy). Engineering Geology 2011;118(1-2):1-9.

Furukawa H, Pichai W. Salt and sinkhole: Corrosion as a principal factor governing topography and mass movement in Northeast Thailand. Japanese Journal of Southeast Asian Studies 1989;27(1):3-34.

Giao PH, Prechavit N, Manop R. Electric modeling and imaging of sinkholes developed after the 26 December 2004 Tsunami in the Karstic Limestone in the Southern Thailand. Proceedings of First EAGE South-East Asia Regional Geology Workshop-Workshop on Palaeozoic Limestones of South-East Asia and South China; 2011 Dec 5-8; Ipoh: Malaysia; 2011.

Gutiérrez F, Parise M, De Waele J, Jourde H. A review on natural and human-induced geohazards and impacts in karst. Earth-Science Reviews 2014;138:61-88.

Heidari M, Khanlari GR, Beydokhti AT, Momeni AA. The formation of cover collapse sinkholes in North of Hamedan, Iran. Geomorphology 2011;132(3-4):76-86.

Kaufmann G, Romanov D, Nielbock R. Cave detection using multiple geophysical methods: Unicorn Cave, Harz Mountains, Germany. Geophysics 2011;76(3):71-7.

Kaufmann G. Geophysical mapping of solution and collapse sinkholes. Journal of Applied Geophysics 2014;111:271-88.

Kaufmann G, Romanov D, Tippelt T, Vienken T, Werban U, Dietrich P, et al. Mapping and modelling of collapse sinkholes in soluble rock: The Münsterdorf site, northern Germany. Journal of Applied Geophysics 2018;154:64-80.

Kidanu ST, Torgashov ET, Varnavina AV, Anderson NL. ERT-based Investigation of a Sinkhole in Greene County, Missouri. AIMS Geosciences 2016;2(2):99-115.

Kruse S, Grasmueck M, Weiss M, Viggiano D. Sinkhole structure imaging in covered karst terrain. Geophysical Research Letters 2006;33(16):Article No. L16405.

Land Development Department. Soil types in Phu Pha Man District [Internet]. 2005 [cited 2023 Feb 20]. Available from: http://oss101.ldd.go.th/web_thaisoilinf/62_soilgroup/62sg_desc/desc_33gm.html/ (in Thai).

Margiotta S, Negri S, Parise M, Valloni R. Mapping the susceptibility to sinkholes in coastal areas, based on

stratigraphy, geomorphology and geophysics. Natural Hazards 2012;62:657-76.

Minezaki T, Hisada KI, Hara H, Kamata Y. Tectono-stratigraphy of late carboniferous to Triassic successions of the Khorat Plateau Basin, Indochina Block, Northeastern Thailand: Initiation of the Indosinian Orogeny by collision of the Indochina and South China blocks. Journal of Asian Earth Sciences 2019;170:208-24.

Nam BH, Kim YJ, Youn H. Identification and quantitative analysis of sinkhole contributing factors in Florida's Karst. Engineering Geology 2020;271:Article No. 105610.

Pando L, Pulgar JA, Gutiérrez-Claverol M. A case of man-induced ground subsidence and building settlement related to karstified gypsum (Oviedo, NW Spain). Environmental Earth Sciences 2013;68:507-19.

Ponta G, Memon B, LaMoreaux J, Julawong J, Wongsawat S. Karst Landforms in the Saraburi Group Limestones, Thailand. Proceedings of the Thirteenth Multidisciplinary Conference on Sinkholes and the Engineering and Environmental Impacts of Karst; 2013 May 6-10; National Cave and Karst Research Institute, Carlsbad, New Mexico: USA; 2013.

Richardson S. Sinkhole and Subsidence Record in the Chuniespoort Group Dolomite, Gauteng, South Africa [dissertation]. Pretoria, University of Pretoria; 2013.

Satarugsa P. The Lessons learnt from geophysical investigation of sinkholes in rock salt in Thailand. Proceedings of International Conference on Geology, Geotechnology and Mineral Resources of Indochina; 2011 Dec 1-3; Khon Kaen: Thailand; 2011.

Sauro F, Mecchia M, Piccini L, De Waele J, Carbone C, Columbu A, et al. Genesis of giant sinkholes and caves in the quartz sandstone of Sarisariñama tepui, Venezuela. Geomorphology 2019;342:223-38.

Theron A, Engelbrecht J. The role of earth observation, with a focus on SAR Interferometry, for sinkhole hazard assessment. Remote Sensing 2018;10(10):Article No. 1506.

Tufano R, Guerriero L, Annibali Corona M, Bausilio G, Di Martire D, Nisio S, et al. Anthropogenic sinkholes of the city of Naples, Italy: An update. Natural Hazards 2022;112(3):2577-608.

Ueno K, Charoentitirat T. Carboniferous and Permian. In: Ridd MF, Barber AJ, Crow MJ, editors. The Geology of Thailand. United Kingdom: Geological Society of London; 2011. p. 71-136.

Upper Northeastern Meteorological Center. Monthly rainfall of Khon Kaen Province by District [Internet]. 2022 [cited 2023 Jan 11]. Available from: http://www.khonkaen.tmd.go.th/rainmet_kk.php/ (in Thai).

United States Geological Survey (USGS). Sinkholes | U.S. Geological Survey [Internet]. 2018 [cited 2023 Feb 15]. Available from: https://www.usgs.gov/special-topics/water-science-school/science/sinkholes/.

Van Den Eeckhaut M, Poesen J, Dusar M, Martens V, Duchateau P. Sinkhole formation above underground limestone quarries: A case study in South Limburg (Belgium). Geomorphology 2007;91(1-2):19-37.

Waltham T, Bell FG, Culshaw MG, Knez M, Slabe T. Sinkholes and subsidence: Karst and cavernous rocks in engineering and construction. Chichester, United Kingdom: Springer-Praxis; 2005.

Watlet A, Kaufmann O, Triantafyllou A, Poulain A, Chambers JE, Meldrum PI, et al. Imaging groundwater infiltration dynamics in the karst vadose zone with long-term ERT monitoring. Hydrology and Earth System Sciences 2018;22(2):1563-92.

Williams P. The role of the epikarst in karst and cave hydrogeology: A review. International Journal of Speleogy 2008;37(1):1-10.

Yordkayhun S. Geophysical characterization of a Sinkhole Region: A study toward understanding geohazards in the Karst Geosites. Sains Malaysiana 2021;50(7):1871-84.

Youssef AM, Al-Harbi HM, Gutiérrez F, Zabramwi YA, Bulkhi AB, Zahrani SA, et al. Natural and human-induced sinkhole hazards in Saudi Arabia: Distribution, investigation, causes and impacts. Hydrogeology Journal 2016;24(3):625-44.

Youssef AM, Zabramwi YA, Gutiérrez F, Bahamil AM, Otaibi ZA, Zahrani AJ. Sinkholes induced by uncontrolled groundwater withdrawal for agriculture in arid Saudi Arabia. Integration of remote-sensing and geophysical (ERT) techniques. Journal of Arid Environments 2020;177:Article No. 104132.

Zhou W, Beck BF, Adams AL. Effective electrode array in mapping karst hazards in electrical resistivity tomography. Environmental Geology 2002;42:922-8.